Thomas Plehn | Jörg Megow | Volkhard May

Concerted charge and energy transfer processes in a highly flexible fullerene–dye system

a mixed quantum–classical study

Suggested citation referring to the original publication:
Phys. Chem. Chem. Phys. 16 (2014), pp. 12949–12958
DOI http://dx.doi.org/10.1039/C4CP01081G
ISSN (online) 1463-9084
ISSN (print) 1463-9076

PCCP

PAPER

View Article Online
View Journal | View Issue

Cite this: *Phys. Chem. Chem. Phys.*, 2014, **16**, 12949

Concerted charge and energy transfer processes in a highly flexible fullerene–dye system: a mixed quantum–classical study

Thomas Plehn,*[a] Jörg Megow[b] and Volkhard May[a]

Received 13th March 2014,
Accepted 7th May 2014

DOI: 10.1039/c4cp01081g

www.rsc.org/pccp

Photoinduced excitation energy transfer and accompanying charge separation are elucidated for a supramolecular system of a single fullerene covalently linked to six pyropheophorbide-*a* dye molecules. Molecular dynamics simulations are performed to gain an atomistic picture of the architecture and the surrounding solvent. Excitation energy transfer among the dye molecules and electron transfer from the excited dyes to the fullerene are described by a mixed quantum–classical version of the Förster rate and the semiclassical Marcus rate, respectively. The mean characteristic time of energy redistribution lies in the range of 10 ps, while electron transfer proceeds within 150 ps. In between, on a 20 to 50 ps time-scale, conformational changes take place in the system. This temporal hierarchy of processes guarantees efficient charge separation, if the structure is exposed to a solvent. The fast energy transfer can adopt the dye excitation to the actual conformation. In this sense, the probability to achieve charge separation is large enough since any dominance of unfavorable conformations that exhibit a large dye–fullerene distance is circumvented. And the slow electron transfer may realize an averaging with respect to different conformations. To confirm the reliability of our computations, ensemble measurements on the charge separation dynamics are simulated and a very good agreement with the experimental data is obtained.

1 Introduction

Within the last few decades fullerene based supramolecular systems have attracted increasing interest with regard to potential application in dye sensitized solar cells and artificial photosynthetic systems.[1–6] Commonly, the fullerenes are integrated in such solar cells in order to promote the basic charge separation processes at the boundary layer after photoexcitation of the dye molecules. Accordingly, a great diversity of studies has been accomplished focusing on details of the excitation energy transfer (EET) as well as the electron transfer (ET) in such artificial systems.[7–13] So far related theoretical investigations either concern rather rigid structures[14–20] or discuss systems being subject to transfer phenomena on the femtosecond time-scale.[10,12,21–27]

The present study considers slower processes where EET and ET may interfere with structural changes in the light absorbing system. Our computations focus on phenomena on a picosecond time-scale in the highly flexible C_{60}–hexapyropheophorbide-*a* (**FP6**) molecular system[28] shown in Fig. 1. Its synthetic protocol and photophysical properties were reported in earlier experimental investigations.[29] The six pyropheophorbide-*a* dyes (Pyropheo) and the single C_{60} fullerene are covalently bound to each other *via* two dendrimeric linker structures. These mainly consist of sp^3-hybridized carbon atoms which barely stabilize the structure of the adduct. As the result the whole **FP6** is subject to continuous conformational changes.

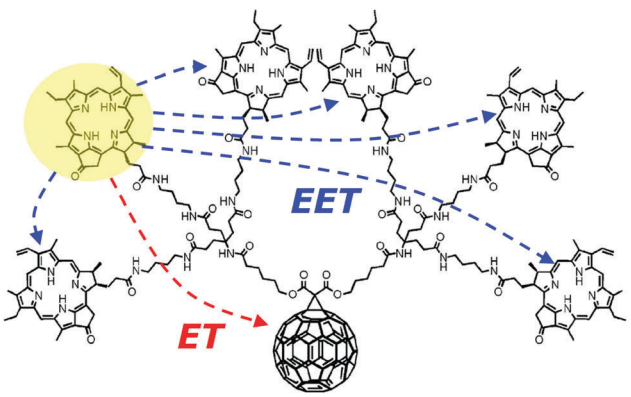

Fig. 1 Structure of **FP6** and the presentation of a possible transfer phenomena starting from an excited Pyropheo (yellow). Blue arrows: excitation energy transfer (EET) to the other Pyropheos and red arrows: electron transfer (ET) to the fullerene.

[a] *Institut für Physik, Humboldt Universität zu Berlin, Newtonstraße 15, D-12489 Berlin, Germany. E-mail: plehn@physik.hu-berlin.de, may@physik.hu-berlin.de*
[b] *Institut für Chemie, Universität Potsdam, Karl-Liebknecht-Straße 24-25, D-14476 Potsdam, Germany*

The initial absorption of visible light takes place at the six Pyropheos. Once excited, EET redistributes the excitation among these molecules. Simultaneously, ET becomes possible from any excited Pyropheo to the fullerene unit. In this way, **FP6** can be regarded as a tiny photosynthetic apparatus realizing light harvesting and charge separation. Accordingly, it becomes of interest as a possible component of a dye-sensitized solar cell. Concerning this issue, the fullerene unit would be covalently anchored or deposited on a semiconductor surface as, for instance, SnO_2 or TiO_2. Attached and under exposure to visible light, the electronically excited dyes give rise to ET to the fullerene and subsequent charge injection into the semiconductor conduction band (an adequate electrolyte solution surrounding the Pyropheos and a counter electrode would account for the necessary recharging of the dyes). Even more suited to application, the construction of dye-sensitized bulk-heterojunction solar cells[30] based on **FP6** structured layers could be envisaged. Thereby, again the direct combination of light harvesting dyes and the electron accepting fullerene is the decisive feature.

In previous studies we already noted that EET processes, like those being of interest here, take place on a 10 ps time-scale.[31] However concerning the concluding charge separation processes, earlier spectroscopic measurements of **FP6** reported about a general time-scale of more than 100 ps.[29] Both mentioned picosecond time-scales justify to model the transfer dynamics in an incoherent picture based on special rates and a coupled set of Pauli master equations.

In view of the dependence of the transfer kinetics on the actual **FP6** geometry and its continuing alternation, we describe the complex by means of classical molecular dynamics simulations. The trajectories deliver both, picosecond time-scale motion of **FP6** and intramolecular vibrations on the femtosecond time-scale. Based on the classical trajectories we calculate the dynamics of the quantum mechanical electronic **FP6** subsystem. Instead of solving time-dependent Schrödinger equations, here the EET processes are directly approached by introducing mixed quantum–classical Förster rates.[32] These rates are determined in using pre-calculated electronic structural data for the first excited Pyropheo states, their related potential energy surfaces (PESs) as well as the electronic ground state structure of **FP6** and the solvent molecules.[32] The ET rates are directly expressed according to the nonadiabatic Marcus theory. In order to parameterize this semiclassical model, we refuge to a dielectric continuum ansatz of the donor–acceptor (D–A) system,[33,34] which has proven itself on frequent occasions.[12,15,20,35,36] Here the latter simplification allows us to compute the ET rate based on the nuclei trajectories in a more ordinary manner.

In contrast to the time-scale of the ET of about 100 ps, we recognized the geometrical changes of similar Pyropheo architectures to occur within only 20 to 50 ps.[31,32,37–39] So, a respective change of the transfer rates has to be considered. Therefore, we introduce time-dependent transfer rates which change in a discrete manner and in this way take note of the conformational fluctuations. In order to validate the results by comparison with measured data taken from ref. 29, we compute the photoinduced charge separation dynamics not only within a single **FP6** but for an ensemble of systems. Accordingly, it is the second intention of this work to describe the ensemble dynamics including a conceived technique of phase space sampling.

2 Equilibrium dynamics of FP6 in solution

The **FP6** is subject to continuous geometry changes. Besides the structure itself, of course, these depend on the installed temperature and pressure of the simulation as well as the kind of solvent. High viscosity or pressure as well as low temperature obviously stabilize the geometry and decelerate the conformational fluctuations and *vice versa*. Here, we apply lab conditions, which means a temperature of 300 K and a pressure of 1 atm, and consider *N,N*-dimethylformamide (DMF) solvent molecules. The detailed simulation protocol is contained in Section 4.2.

2.1 Dynamics of a single FP6

Fig. 2 shows a snapshot of a **FP6** dissolved in DMF. It gives an impression of the structure flexibility. For a quantitative discussion and a deeper insight into the conformational motion, we determined the possible distances among the seven functional **FP6** units. A simulation is carried out for 150 ps starting from the snapshot visualized in Fig. 2. From the resulting trajectory we obtain the center-to-center distance among, for instance, the fullerene and the Pyropheo 4 (both colored in red in Fig. 2) as well as the Pyropheo 1 and 6 (both colored in blue in Fig. 2). Respectively, the time-dependent fluctuations of both distances are shown in Fig. 3 colored in red (dashed) and blue. The fullerene and the Pyropheo 4 seem to depart continuously from each other (on average about 1 Å/50 ps). On the other hand, Pyropheo 1 and 6 stay at a rather constant distance for about 50 ps until both molecules apparently depart from each other and increase their distance by about 2 Å within the following 5 ps

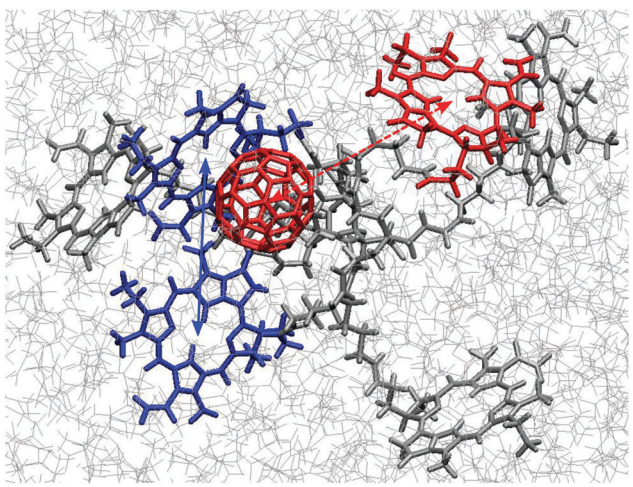

Fig. 2 Snapshot of the dissolved **FP6**. Different parts are visualized: DMF molecules (light grey); Pyropheo 4 and fullerene unit (red); Pyropheo 1 and 6 (blue); remaining **FP6** structure (dark grey); center-to-center distances among the colored subunits are indicated by the red dashed (14.6 Å) and blue (11.7 Å) arrows, respectively.

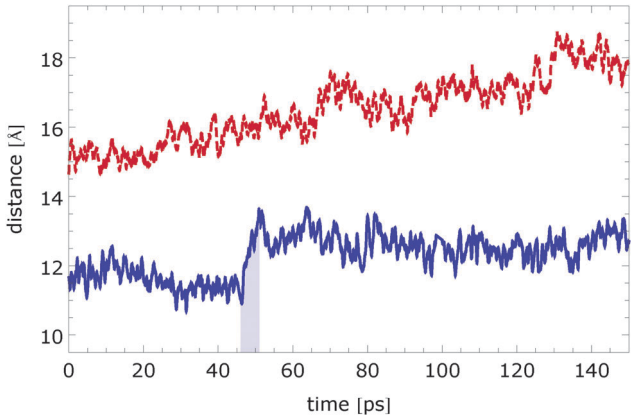

Fig. 3 Time-dependence of a fullerene–Pyropheo (red dashed) and a Pyropheo–Pyropheo (blue) center-to-center distance by way of using two pairs. The fluctuation is taken from a 150 ps simulation. Its initial conformation and the particular tracked molecule pairs are visualized, respectively, colored in Fig. 2.

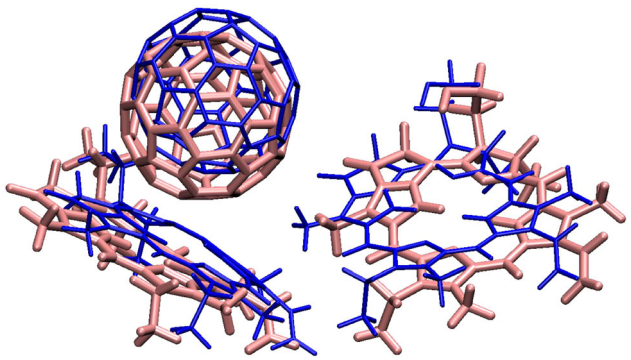

Fig. 4 Relative conformation of the fullerene, Pyropheo 1 (left) and Pyropheo 6 (right) at the beginning (thin blue) and end (thick pink) of the 5 ps interval marked light blue in Fig. 3.

(light blue highlighted in Fig. 3). The molecular structures in Fig. 4 show the relative orientation of Pyropheo 1 (left), Pyropheo 6 (right) and the fullerene at the beginning (thin blue) and end (thick pink) of the particular 5 ps interval. We attribute this special displacement of Pyropheo 1 and 6 to a general affinity for the fullerene and the dyes to align in a face-to-face stacking (*cf.* Section 2.2). As illustrated in Fig. 4, the fullerene "pushes" both Pyropheos apart in order to promote such π–π stacking with Pyropheo 1. This causes the abrupt separation of the dyes. After this sudden motion, their distance fluctuates again in the usually temperate manner. However, since these "tri-relations" are rather unlikely such fast conformational changes are also observed very infrequently.

In this sense, we generally suggest that the conformation of the **FP6** system cannot be assumed to stay fixed on a time-scale above 50 ps. But, on the 10 ps time-scale the structure seems to be approximately constant.

2.2 Dynamics of a FP6 ensemble

To study the equilibrium properties of **FP6** in solution, we created an ensemble of equilibrated systems. The performed phase space sampling and simulation procedure are described in Section 4.2. By means of 120 pre-equilibrated trajectories (each of 150 ps length), an insight is obtained into the equilibrium ensemble statistics. In particular, we studied the distances among all the 15 Pyropheo pairs as well as between each of the six Pyropheos and the fullerene. For this purpose, we analyzed all $120 \times 150 \times 1000 = 1.8 \times 10^7$ **FP6** conformations at hand (1 fs time-steps). Received from each of the 1.8×10^7 conformations, all 15 Pyropheo–Pyropheo and all six fullerene–Pyropheo pairs are listed together and summarized according to their realized center-to-center distances.

The count of both kinds of distances is presented in Fig. 5 by the blue and red lines, respectively. Both curves are normalized to their maximum values. As shown, inter-Pyropheo distances of about 19–28 Å are found most frequently. Distances less than 8 Å and more than 38 Å occur only rarely. Taking this finding, we conclude that the six dyes within **FP6** tend not to build dimer structures in DMF solution. Moreover, the upper distance limit simply reflects the range of the dendrimer linkers. The red colored distribution in Fig. 5 reveals the minimum fullerene–dye distance to be about 5.5 Å (center-to-center). Including the radii of the fullerene this represents both molecules in van der Waals contact as, for instance, illustrated in the inset of Fig. 6, where besides the bond structure the van der Waals spheres of the individual atoms are also imaged.

Moreover, the red distribution in Fig. 5 shows a peak at rather small fullerene–dye distances of about 6.2 Å. It points out a relatively high probability of closely arranged fullerene–dye pairs. However, such a peak does not appear in the blue dye–dye distribution curve at a comparable distance. This latter observation seems to be reasonable considering the side groups of the dye molecules. In fact, the Pyropheo–Pyropheo "approaching" is sterically hindered by their dangling sidegroups. In the case of the face-to-face ("ball-on-plate") aligned fullerene–dye pairs, on the other hand, the dye sidegroups do not block their "approaching" because of the smaller size of the fullerene.

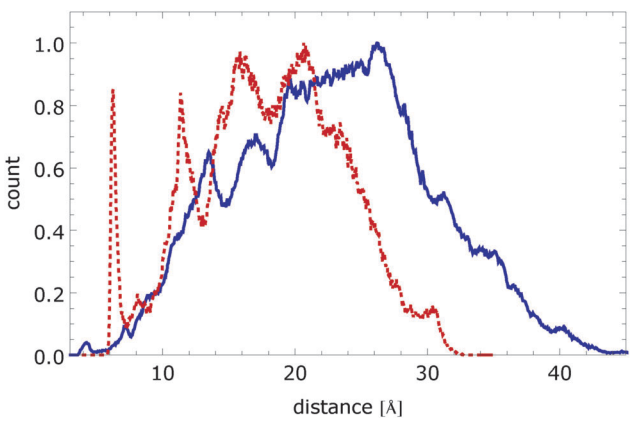

Fig. 5 Normalized molecule–molecule distance distributions within the equilibrated ensemble of **FP6** dissolved in DMF. Shown are the relative count of all Pyropheo–Pyropheo pairings (blue full line) and fullerene–Pyropheo pairs (red dashed line) against their respective molecule–molecule (center-to-center) distances.

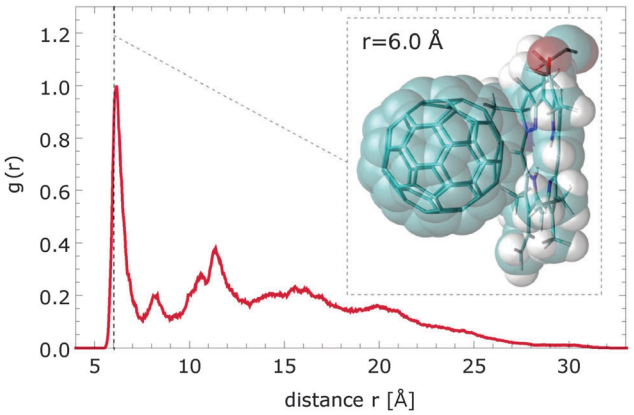

Fig. 6 Normalized radial distribution function $g(r)$ of Pyropheo molecules around the fullerene against the Pyropheo–fullerene distance r. Inset: π–π stacked (face-to-face) fullerene–Pyropheo apposition taken from a sample snapshot describing a center-to-center distance of about 6.0 Å.

As the result, these latter π–π stackings are much more stable with respect to the dye–dye stackings.

The dominant affinity for the six Pyropheos to approach the fullerene becomes even more striking, when concerning the main panel of Fig. 6. It shows the radial distribution function $g(r)$ of dye molecules located in distance r around the fullerene. Similar to the red curve in Fig. 5, the $g(r)$ results by including all six fullerene–dye pairs (by default $g(r)$ accounts for the radially increasing sphere volume around the fullerene center). Additionally, Fig. 6 presents $g(r)$ normalized to the maximum value.

The observed oscillations of $g(r)$ reveal successive regions of higher and lower dye density. In general, such oscillating behavior can be interpreted as the tendency of the dyes to become arranged in shells or layers around the fullerene. In this sense, the first highest density peak at r = 6.2 Å clearly testifies the affinity for the Pyropheos to accumulate at the fullerene. This latter fact is reasonable since, besides their sterically unhindered approaching, the π–π stacked face-to-face attachment seems energetically very favored. In fact, the large-area contact in the van der Waals distance (see inset of Fig. 6) gives rise to a lower potential energy by contrast with the situation of the fullerene and dye each individually surrounded by only DMF molecules. And, consequently, after the initial system equilibration phase, such stacked dye–fullerenes are realized with, respectively, high probability within the ensemble. Beyond the distance of 7.5 Å (first minimum of the red line in Fig. 5), obviously the DMF molecules seem to start penetrating between the arranged molecules and the conformation loses its stability and preference.

In accordance with reports about similar fullerene–porphyrin complexes, the π–π stacking was defined by a fullerene–Pyropheo center-to-center distance smaller than 7.0 Å.[12] Using this we computed that a percentage of about 20.2% of all **FP6** conformations realizes such a stacking in DMF solution. In other words, about 3.4% of all fullerene–Pyropheo pairings. Even though the probability of 3.4% is rather small concerning all possible distances, it is remarkably high with respect to the probability of face-to-face dye–dye stacking. Namely, a comparable study of the dye–dye distances states that only less than 0.1% of the Pyropheo–Pyropheo pairs in **FP6** arrange in π–π stackings.

3 Concerted excitation energy and electron transfer

Due to the time-scale of ET the coupled EET and ET dynamics are considered on a 150 ps time interval. As already indicated the **FP6** structure undergoes pronounced changes within such a 150 ps interval. However, in very good approximation the **FP6** structure can be assumed to stay fixed on a 10 ps interval. Accordingly, it is not possible to compute single transfer rates which represent the full interval of 150 ps. Instead we must take advantage of the 10 ps time-scale. This conceptional precondition comes along with introducing rates of Förster and Marcus types. Arising from Fermi's golden rule, both simply assume constant transfer couplings and thus do not account for the critical overall **FP6** conformational motion.

Therefore, we subdivided the 150 ps trajectory into 15 subsequent slices of each 10 ps length. These subintervals allow for the proper calculation of 15 individual sets of rates. Considering the different transfer processes each of these sets contain 30 EET and 6 ET rates, which are only valid for the respective 10 ps of nuclear dynamics. So, in total, a sequence of 15 rate sets results. Aligned in a proper chronological order, the latter sequence of constant rates gives rise to a single discrete time-dependent set of rates for the complete 150 ps interval. Every 10 ps the transfer dynamics are described by a new set of transfer rates, representing the changed **FP6** conformation. Moreover, it is important to note that the steplike changes in the individual rates are responsible for discontinuities of the transfer processes, if concerning only a single-**FP6** kinetics. However, here these are finally averaged out when considering the ensemble dynamics.

3.1 Conformation-dependent transfer rates

The here utilized mixed quantum–classical approach of the electron dynamics is based on the so-called Ehrenfest dynamics in combination with the ground state classical path approximation.[40] The electronic system of the full **FP6** is reduced to its seven functional units.[31,32,37–39] Only electronic transitions among the six Pyropheos and the fullerene unit are of interest. Furthermore, the electronic **FP6** states are represented in terms of a direct-product of the respective seven adiabatic single-molecule states. Such an approach is reasonable due to a negligible overlap of the wave functions corresponding to different subunits.[32] The mth excited **FP6** state, for instance, is built up by the first excited-state wavefunction of the mth Pyropheo and the six ground state wave functions of the remaining Pyropheos and the fullerene. In this way the possible excited **FP6** states are limited to only single excitations. We furthermore concern neither ET processes among the Pyropheo molecules nor should the fullerene participate in the EET. Also the initial excitation is not treated in terms of the interaction of molecular transition dipole moments with an externally applied electric field as, for instance, shown in ref. 39.

Instead, the **FP6** excitation is simply introduced in terms of the initial condition of the finally computed dynamics.

3.1.1 Rate of EET. For calculating the EET rates, firstly, the excitation energies of the six **FP6** states are required. The respective six potential energy gaps corresponding to the individual Pyropheo sites are denoted as

$$U_{meg}(X) = E_{eg} + \Delta U_{meg}^{(intra)}(R_m) + \Delta U_{meg}^{(inter)}(X). \quad (1)$$

The energy gap function $U_{meg}(X)$ describes the energy of the excited mth Pyropheo (within its specific environment) with respect to the corresponding ground state energy. The first term E_{eg} indicates the pure electronic Pyropheo excitation energy (so-called 0–0 transition). The second term $\Delta U_{meg}^{(intra)}(R_m)$ denotes the difference in the intramolecular PESs corresponding to the mth Pyropheo excited- and ground states. Respectively, the third term $\Delta U_{meg}^{(inter)}(X)$ in eqn (1) accounts for the energy difference, which results from the interaction between the mth Pyropheo and its environment. The sets R_m and X cover only the nuclear coordinates of the mth Pyropheo unit and all nuclear coordinates within the system, respectively. While the excitation energy is defined as a constant of E_{eg} = 1.86 eV,[32] the PESs as well as their intermolecular interactions of course depend on the present nuclear position coordinates. Here, we approach the intramolecular PESs in harmonic approximation. A detailed description can be found in our earlier studies.[31,32] In course of these previous studies the necessary Hessian matrices and the respective equilibrium reference nuclear coordinates were already calculated.

The intermolecular interaction, on the other hand, is obtained in terms of Coulomb interactions[41] following the general expression

$$J_{mn}(ab, cd) = (1 - \delta_{mn}) \sum_{\mu,\nu} \frac{q_{m\mu}(ad) q_{n\nu}(bc)}{|\mathbf{R}_{m\mu} - \mathbf{R}_{n\nu}|}. \quad (2)$$

Concerning two particular molecules m and n in the electronic states a and b, respectively, their interaction can be expressed as J_{mn}(ab,ba) among two sets of the so-called atomic centered partial (point) charges $\{q_{m\mu}(aa)\}$ and $\{q_{n\nu}(bb)\}$. The coordinates $\mathbf{R}_{m\mu}$ and $\mathbf{R}_{n\nu}$ represent the positions of the atoms μ and ν in molecules m and n, respectively. Each set of charges refers to a certain kind of molecule and electronic state. The sets required here, which represent the ground states of all molecules and the excited Pyropheo state themself, are computed in preparation as explained in Section 4.1.

Next, the excitonic coupling J_{mn}(eg,eg) between two Pyropheos m and n is required. As the excitation energies the coupling expressions J_{mn}(eg,eg) are time-dependent due to their dependencies on the atomic position coordinates of the Pyropheos. It is formulated by analogy with the intermolecular Coulomb interaction based on the general Coulomb expression J_{mn}(ab,cd), eqn (2), but utilizing the so-called atomic centered partial transition charges with a, c = g and b, d = e, instead of the usual static point charges.[41] The respective set of pre-calculated transition charges of the Pyropheos was obtained from earlier studies.[31,32]

Based on a particular 10 ps trajectory and using the quantities of $U_{meg}(X)$ and J_{mn}, both calculated for every individual time-step, we arrive at the mixed quantum–classical expression of the rate of EET from Pyropheo m to n:[32]

$$k_{m\to n} = \frac{2}{\hbar^2} |\bar{J}_{mn}|^2 \mathrm{Re}\left\{ \int_0^T \mathrm{d}\tau \left\langle \mathrm{e}^{-i\eta_n(\tau,0)} \right\rangle \left\langle \mathrm{e}^{i\eta_m(\tau,0)} \right\rangle \right\}. \quad (3)$$

The $\bar{J}_{mn}$ represents the excitonic coupling averaged with respect to the complete trajectory (10 000 time-steps á 1 fs). Such averaging is reasonable since only small fluctuations of J_{mn} take place on time-scales of about 10 ps.[31] In order to derive eqn (3), the usual Fermi's golden rule rate is translated into the dynamical classical limit.[31] Accordingly, the classical functions $\eta_m(\tau, 0) = \int_0^\tau \mathrm{d}t U_{meg}(t)/\hbar$ are introduced, which include the dependence on the PES differences U_{meg}. The angular brackets $\langle \ldots \rangle$ arise from the expectation value with respect to the ground state related vibrational motion of the Pyropheos. Here, we employed the ground state classical path approximation to replace the original expectation value corresponding to the nuclear motion according to the mth excited state. The given factorized modification in eqn (3) can be used due to the assumed vibrational uncorrelation of the six Pyropheo molecules.[31,32,39] Moreover, we found in similar studies that the expressions $\langle \exp\{-\eta_n(\tau,0)\} \rangle$ and $\langle \exp\{\eta_m(\tau,0)\} \rangle$ already converge to zero within about 100 fs. This enables us to calculate both expectation values by means of a simple averaging with respect to 100 subintervals each of T = 100 fs. The basic 100 subintervals are obtained by equally dividing the 10 ps trajectory. And according to this, the upper integation limit in eqn (3) is reduced to 100 fs.

3.1.2 Rate of ET. In principle, it would also be possible to derive an ET rate similar to eqn (3). However, here the ET rates are calculated in a less expensive manner following the semiclassical Marcus theory.[33] This model of nonadiabatic type is motivated by the assumed weak electronic coupling. It is combined with the so-called "two-sphere" (Rehm–Weller) model.[15,20,34] Instead of accounting for the atomic structure it treats the Pyropheo–fullerene (D–A) system in terms of two isotropic charged spheres separated by the distance d_m and surrounded by a continuous medium.

For calculating the rate of ET from the mth Pyropheo to the fullerene, the reaction free-energy ΔF_m^0, the reorganization free-energies λ_m as well as the transfer integrals V_m are required. The dielectric continuum model delivers $\Delta F_m^0 = e(E^{(ox)} - E^{(red)}) - e^2/\varepsilon_s d_m - E_{eg}$ with dependence on the D–A distance d_m.[12,34,36] Referencing from the literature, we chose the parameters according to $E^{(ox)}$ = 0.42 eV,[42] $E^{(red)}$ = −0.63 eV[43] and ε_s = 37.0 indicating the oxidation potential of the Pyropheo, the reduction potential of the fullerene and the dielectric constant of DMF, respectively. Also the reorganization free-energy follows the two-sphere model with simple dependence on d_m by $\lambda_m = e^2(1/n^2 - 1/\varepsilon_s)(1/2r_{P^+} + 1/2r_{F^-} - 1/d_m) + \lambda^{(intra)}$.[35,36,44,45] The additional system parameters denote the refraction index of DMF n = 1.43, the effective radii of the cationic Pyropheo r_{P^+} = 4.4 Å and the anionic fullerene unit r_{F^-} = 4.0 Å as well as the parameter $\lambda^{(intra)}$ = 0.3 eV. Their particular values were already estimated in the course of the previous **FP6** study.[29] The latter parameter $\lambda^{(intra)}$ accounts for reorganization along the possible

intramolecular vibrational modes of the mth Pyropheo and the fullerene.[44,46] The additionally required transfer integrals are obtained using the typical approximate expression $V_m = V^{(0)} \cdot \exp\{-\beta(d_m - d^{(0)})\}$, which approaches the characteristic exponential decrease of the molecular orbital overlap at a magnifying fullerene–dye distance.[47–49] Similar to ΔF^0_m and λ_m, V_m simply depends on the D–A separation d_m. The parameters $V^{(0)}$ = 100 cm^{-1}, $d^{(0)} = r_{P^+} + r_{F^-}$ = 8.4 Å and β = 0.5 Å^{-1} are used to modulate the exponential decay. In ref. 29, the particular values were introduced based on different ET studies of comparative fullerene based D–A systems. The $V^{(0)}$ was approximately chosen with regard to the introduced minimum distance $d^{(0)}$. Accordingly, we started our computation by maintaining this value of $V^{(0)}$ = 100 cm^{-1}. However, after the confrontation of our final results with the experimental data (*cf.* Section 5), instead a larger coupling parameter $V^{(0)}$ = 160 cm^{-1} appears to be more appropriate. This correction by the factor 1.6 seems arbitrary, but becomes reasonable concerning the high sensitivity of $V^{(0)}$ for not only the fullerene–dye separation but also their relative orientation. Guldi *et al.* reported about these dependencies by studying comparable fullerene–porphyrin architectures.[9] In fact, their semiempirical molecular orbital calculations unveiled that the electronic coupling of a face-to-face (π–π stacked) alignment (415 cm^{-1})[50] can exceed the coupling of the identical D–A pair in face-to-edge orientation (59 cm^{-1})[50] by as much as a factor of ∼7.

In order to model again a constant rate representing a certain 10 ps interval, we introduce the distance $\bar{d}_m$ which is averaged with respect to the complete 10 ps. The averaged distance $\bar{d}_m$ is further utilized for computing the parameters $\Delta F^0_m(\bar{d}_m)$, $\lambda_m(\bar{d}_m)$ and $V_m(\bar{d}_m)$. Finally, the Marcus rate $r_{m\to F}$ takes the following form (T = 300 K)

$$r_{m\to F} = \frac{|V_m(\bar{d}_m)|^2}{\hbar}\sqrt{\frac{\pi}{k_B T \lambda_m(\bar{d}_m)}} \times \exp\left\{\frac{-(\Delta F^0_m(\bar{d}_m) + \lambda_m(\bar{d}_m))^2}{4k_B T \lambda_m(\bar{d}_m)}\right\}. \quad (4)$$

In the fashion of the EET rate, eqn (3), the introduced averaged parameters give rise to time-independent but conformation-specific ET rates.

According to eqn (4), it is apparent that the ET rate depends only on the D–A distance. In principle, this means that it would also be possible to compute an ET rate based on individual time steps without the above averaging. Although conceptually highly questionable, we followed this alternative approach to elucidate, by way of an example, how the constant rates, eqn (4), are applied for calculating the transfer dynamics for a 150 ps interval. Again, the already considered fullerene–Pyropheo distance fluctuation, which is given by the red dashed line in Fig. 3, may serve as the example here. The discrete alternation of the 15 constant ET rates is given by the black line in Fig. 7. They follow from an application of eqn (4) each on the 15 subsequent 10 ps intervals. For comparison the rates based individually on each frame are presented by the red line.

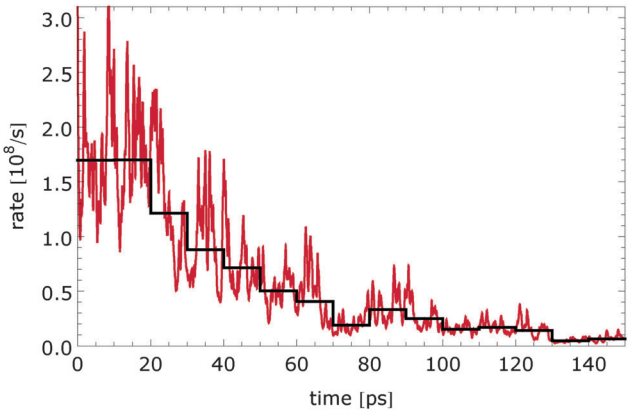

Fig. 7 Descrete time-dependence of the ET rate. Red line: ET rate directly computed for the fluctuating fullerene–dye distance. Black line: ET rates each averaged with respect to a 10 ps interval (*cf.* eqn (5)). Distance fluctuation is taken from the red dashed line in Fig. 3.

The scope of validity of each of the individual constant rates is only the corresponding basic 10 ps interval. In this sense, the steplike black line illustrates the introduced discrete time-dependence of the transfer rates required for computing the kinetics of the full 150 ps length. The continuous departure of the fullerene and the Pyropheo (linearly increasing distance as shown in Fig. 3) can be identified here in terms of a rather exponential decrease of both kinds of rates. In general, such exponential behavior is reasonable concerning the dominant character of the transfer integral. Similarly a stronger amplitude of the fast fluctuations of the ET rate (red line in Fig. 7) is observed at generally smaller D–A distances.

3.2 Transfer dynamics and ensemble kinetics

Finally, the transfer dynamics within the **FP6** are obtained by solving the following set of coupled Pauli master equations

$$\partial_t P_m(t) = -r_{m\to F}(t)P_m(t) + \sum_{n\neq m}^{6}[k_{n\to m}(t)P_n(t) - k_{m\to n}(t)P_m(t)]$$
$$\partial_t R_m(t) = r_{m\to F}(t)P_m(t). \quad (5)$$

The $P_m(t)$ and $R_m(t)$ indicate the population of the mth electronic excited- and the mth charge separated **FP6** state, respectively. The resulting dynamics shall proceed from t = 0 up to t = 150 ps. Besides the continuous time-dependence of the populations, the discussed discrete time-dependence of the transfer rates (see Fig. 7) is also denoted in eqn (5). After every 10 ps the set of total 36 rates is changed regarding the changed **FP6** geometry. The respective new set is introduced resulting from the next 10 ps of the nuclear motion and the solution of the rate equations proceeds from the final populations of the foregoing 10 ps interval. In this way, the electronic dynamics gradually take note of the crude motion of the structure.

3.2.1 Photoinduced charge separation in the FP6 ensemble. In order to validate our computations, we look for the comparison with appropriate experimental data. The **FP6** was studied

when dissolved in DMF solution.[29] The investigation was based on cw-absorption as well as picosecond transient absorption measurements. With the latter technique the depopulation of the excited **FP6** states after an initial absorption process can be directly sampled. In general a lot of quenching processes are conceivable which would result in such population decay. But concerning the **FP6**, the experimental study unveiled that the ET processes are the most effective depletion channels. In this sense, the depopulation represents the photoinduced charge separation process, which can be easily calculated in terms of the total population of the six excited **FP6** states by utilizing eqn (5). However, the related data were not obtained *via* single molecule spectroscopy but are the result of an ensemble measurement. Now, differently realized **FP6** conformations as well as different initial excitations contribute to the overall signal. Consequently, the calculated dynamics must also be averaged with respect to an ensemble of different geometries and initial excitations.

For this purpose, we actually conceived the phase space sampling as detailed in Section 4.2 (see also the foregoing section). It finally results in an ensemble of 120 pre-equilibrated **FP6** conformations. Starting from each of these 120 conformations, we individually simulate the nuclear dynamics for 150 ps and further calculate the respective 120 sets of transfer rates. Moreover, we introduce six possible initial excitations in terms of the single-Pyropheo excitations. Concerning the generally weak excitonic coupling among the Pyropheos any initially delocalized excitation can be neglected. The coupled rate equations, eqn (5), are solved 6 × 120 = 720 times, by using the 120 rate sets and by applying each the six different initial excitations. Once all 720 population dynamics are generated the photoinduced charge separation within the ensemble can be characterized by the expression

$$\mathscr{P}(t) = \frac{1}{120}\sum_{s=1}^{120}\frac{1}{6}\sum_{i=1}^{6}\left(\sum_{m} P_m(t;s,i)\right). \qquad (6)$$

The parameters s and i consider the dependence of the single kinetics on the nuclear dynamics and the initial excitation of the corresponding **FP6** system, respectively. While the summation with respect to the six excited states (m) accounts for the calculation of the total excited state population dynamics, the summations outside the bracket represent the essential averaging procedure.

4 Computational details

4.1 Electronic structure calculations

All electronic ground state structure computations are performed using density functional theory (DFT) methods. The B3LYP exchange correlation functional[51] and a 6-311G(p,d) basis set are chosen as implemented in the GAUSSIAN09 software suite.[52] Moreover a polarizable continuum model adapted to DMF is set up for separately calculating all the atomic centered partial charges by utilizing the ChelpG method.[53] The ground- and first excited state related Hessian matrices and nuclear equilibrium configurations for the Pyropheo molecule as well as its atomic centered partial transition charges[54] are obtained earlier using linear response time-dependent DFT (TD-DFT) methods also employing the GAUSSIAN09 tool. The detailed discussion of modeling the intramolecular PESs of the Pyropheos and its time-dependent description based on nuclear trajectories is presented in ref. 55.

4.2 Simulation technique and phase space sampling

Here, the **FP6** is simulated in the presence of 2897 *N*,*N*-dimethylformamide (DMF) molecules. The simulation box is initially created using the LEAP software tool included in the AMBER 8.0 program.[56] All the molecular dynamics simulations are executed using the NAMD package[57] applying the PARM99 and GAFF force field parameters.[58,59] Resembling lab conditions, the production simulation runs under NPT conditions utilizing Langevin temperature control[60] and Nosé–Hoover Langevin piston pressure control,[61] which retain the system at room temperature of 300 K and a pressure of 1 atm.

The phase space sampling technique for constructing a reliable ensemble of systems is implied by means of multiple distributed high-temperature simulations starting from a single **FP6** comformation. One-eighth of the whole heating → annealing → equilibrating process is visualized in Fig. 8. Each of the red arrows indicate a 2000 K simulation path of 200 ps length; the orange arrows represent the simulated annealing-processes from 2000 K to the achieved 300 K for 50 ps; the thin blue arrows typify the subsequent equilibration-simulations for further 100 ps; and the thick blue arrows describe the final 300 K production-runs of 150 ps length. Due to the implemented 2000 K-phases, the initial conformations of the individual production-runs can be assumed to be distributed far apart in the phase space. Executed for eight times in a similar manner, the whole processing gives rise to 8 × 15 = 120 trajectories (which means 15 trajectories in Fig. 8).

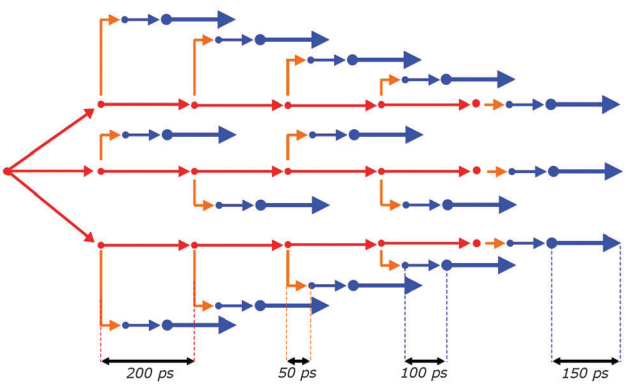

Fig. 8 Scheme of the phase space sampling procedure. Only one of the eight similar processes or "simulation branches" is shown. Points: system states; red arrows: 2000 K heat trajectories of 200 ps length; orange arrows: 2000 → 300 K annealing trajectories of 50 ps length; thin blue arrows: 300 K equilibration trajectories of 100 ps length; and thick blue arrows: 300 K production trajectories of 150 ps length. Subsequent arrow head and tails are connected by the identical atomic position coordinates of the system.

5 Results

Fig. 9 displays different ensemble kinetics of charge separation in comparison to the experimental data.[29] The latter are given by the blue points. The blue dashed line arises from the calculations, eqn (6), in the usual manner by computing the EET and ET rates using eqn. (3) and (4) together with the parameters as defined above. Also the green full line results from the coupled EET and ET dynamics, however here we applied a generally increased transfer integral by using $V^{(0)}$ = 160 cm^{-1} instead of the reference value $V^{(0)}$ = 100 cm^{-1}. In general, $\mathscr{P}(0)$ = 1.0 indicates that a single excitation is initially present in **FP6**. Then, $\mathscr{P}(t > 0) < 1.0$ results from the probability outflow by means of the ET processes. In particular, the ensemble kinetics resulting from the larger $V^{(0)}$ agree very well with the experimental data. Here, it is necessary to mention that the general disagreement within the initial 20–25 ps in Fig. 9 should not be subject to the comparison. Namely, the measurements were performed using laser pulses of about 20 ps width. This means, within about the initial 20 ps the measured data are fraught with technical difficulties and a certain degree of inaccuracy has to be assumed. Moreover, it is important to remind that the calculated dynamics describe an ensemble averaged and multi-exponential population decay. So, the achieved agreement must not be directly attributed to the increased strength of the transfer integral. Instead, it demonstrates the quality of the here constructed ensemble and the suitable usage of the time-dependent rate ansatz.

In general, all transfer cascades of the photoinduced charge separation can be distinguished according to the contribution of any EET processes. Either the ET takes place directly from the initially excited Pyropheo to the fullerene, or it starts from any other Pyropheo which becomes excited by means of intermediate EET processes. In order to study the role of the indirect type of transfer, we repeated the calculations of the dynamics $\mathscr{P}(t)$, eqn (6), without any EET processes ($k_{m\to n}$ = 0). The resulting dynamics of only direct charge separation are presented in Fig. 9 by the red dashed line. Its comparison with the other curves and the experimental data shows a strong difference, which emphasizes the fundamental role of the transfer cascades *via* intermediate EET. In this sense, the kinetics of photoinduced charge separation cannot be described as a pure ET phenomenon, but indeed necessarily require the simultaneous treatment of the EET and ET processes. On the other hand, if the ET processes are typically as fast as (or even faster than) the EET processes, the single direct ET pathway would dominate the charge separation. However, such high ET rates of $r_{m\to F} > 10^{12}$ s^{-1} are only achievable by D–A distances of about <8.5 Å (see eqn (4)). And in fact, we found that only less than 1% of all Pyropheos would be both initially excited as well as positioned in sufficiently close proximity to yield the respective ET strength. Regarding this small percentage, the different EET processes are obviously needed to, first of all, redistribute the initial excitation over all six Pyropheos. In other words, the EET submits the most efficient channel of charge separation – independently on the present **FP6** conformation.

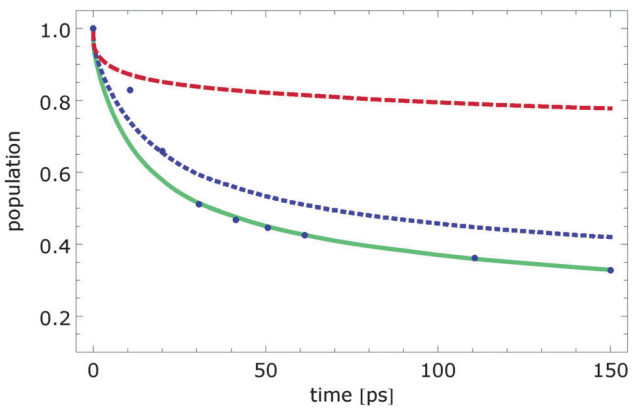

Fig. 9 Ensemble averaged transfer dynamics according to $\mathscr{P}(t)$, eqn (6). Calculations have been carried out by including EET processes and using the transfer integral $V^{(0)}$ = 100 cm^{-1} (blue dotted line) as well as $V^{(0)}$ = 160 cm^{-1} (green full line). Dynamics neglecting the EET processes and by taking $V^{(0)}$ = 160 cm^{-1} are also shown (red dashed line). Blue points display the data based on spectroscopic measurements.

6 Conclusions

Coupled excitation energy transfer (EET) and electron transfer (ET) processes were studied in the highly flexible fullerene dye architecture **FP6** dissolved in an organic solvent. Due to the slow transfer phenomena, the kinetics were computed for a rather long interval of 150 ps. In accordance with the weak electronic couplings, we utilized an incoherent description of the transfer processes in terms of a coupled set of Pauli master equations including mixed quantum–classical EET and semiclassical ET rates based on molecular dynamics simulations. Due to the crude nuclear motion of the system on the 20–50 ps time-scale, a model using discrete time-dependent rates was introduced. In this way, the slow coupled EET/ET dynamics were maintained with dependence on the present **FP6** geometry and taking heed of the continuous conformational variation. Finally, the photoinduced charge separation processes within a **FP6** ensemble were calculated after employing a special phase space sampling technique. The results could be compared with the existing experimental data. We obtained a very good agreement with the measurements. In the first place, this underlines the quality of our incoherent transfer model based on discrete time-dependent mixed quantum–classical rates. By means of the introduced time-dependence the approach circumvented the violation of the basic golden rule assumption of a constant transfer coupling. Moreover, it was proved that the concerted treatment of the transfer processes are vital to the proper description of the photoinduced charge separation. To monitor the particular role of transfer cascades including EET, we additionally computed the kinetics by only taking the direct ET processes into account. The final outcome showed the tremendous importance of the ongoing process of energy redistribution among the six Pyropheos. In particular, the EET phenomena "release" conformation dependent "trapped" excitations, which are only subject to very slow direct ET to the fullerene. In this sense, the EET processes significantly enhance the effective charge separation in the system.

Acknowledgements

Financial support by the *Deutsche Forschungsgemeinschaft* through the project Ma 1356/10–3 is gratefully acknowledged.

References

1 B. O'Regan and M. Grätzel, *Nature*, 1991, **353**, 737–740.
2 D. Gust, T. A. Moore and A. L. Moore, *Acc. Chem. Res.*, 2001, **34**, 40–48.
3 M. Freitag and E. Galoppini, *Energy Environ. Sci.*, 2011, **4**, 2482–2494.
4 A. Yella, H.-W. Lee, H. N. Tsao, C. Yi, A. K. Chandiran, M. Nazeeruddin, E. W.-G. Diau, C.-Y. Yeh, S. M. Zakeeruddin and M. Grätzel, *Science*, 2011, **334**, 629–634.
5 J. Gong, J. Liang and K. Sumathy, *Renewable Sustainable Energy Rev.*, 2012, **16**, 5848–5860.
6 V. Garg, G. Kodis, P. A. Liddell, Y. Terazono, T. A. Moore, A. L. Moore and D. Gust, *J. Phys. Chem. B*, 2013, **117**, 11299–11308.
7 N. S. Sariciftci, L. Smilowitz, A. J. Heeger and F. Wudl, *Science*, 1992, **258**, 1474–1476.
8 N. Martín, L. Sánchez, B. Illescas and I. Pérez, *Chem. Rev.*, 1998, **98**, 2527–2548.
9 D. M. Guldi, *Chem. Soc. Rev.*, 2002, **31**, 22–36.
10 T. L. J. Toivonen, T. I. Hukka, O. Cramariuc, T. T. Rantala and H. Lemmetyinen, *J. Phys. Chem. A*, 2006, **110**, 12213–12221.
11 H. Tamura, I. Burghardt and M. Tsukada, *J. Phys. Chem. C*, 2011, **115**, 10205–10210.
12 R. R. Zope, M. Olguin and T. Baruah, *J. Chem. Phys.*, 2012, **137**, 084317.
13 C. A. Rozzi, S. M. Falke, N. Spallanzani, A. Rubio, E. Molinari, D. Brida, M. Maiuri, G. Cerullo, H. Schramm, J. Christoffers and C. Lienau, *Nat. Commun.*, 2013, **4**, 1602.
14 A. Warshel, *Acc. Chem. Res.*, 2002, **35**, 385–395.
15 A. Amini and A. Harriman, *J. Photochem. Photobiol., C*, 2003, **4**, 155–177.
16 H. M. Correia and M. M. Ramos, *Mater. Sci. Eng., C*, 2005, **25**, 682–686.
17 J. Blumberger, *Phys. Chem. Chem. Phys.*, 2008, **10**, 5651–5667.
18 D. N. LeBard, V. Kapko and D. V. Matyushov, *J. Phys. Chem. B*, 2008, **112**, 10322–10342.
19 V. Tipmanee, H. Oberhofer, M. Park, K. S. Kim and J. Blumberger, *J. Am. Chem. Soc.*, 2010, **132**, 17032–17040.
20 T. Liu and A. Troisi, *J. Phys. Chem. C*, 2011, **115**, 2406–2415.
21 I. Kondov, H. Wang and M. Thoss, *Int. J. Quantum Chem.*, 2006, **106**, 1291–1303.
22 H. Oberhofer and J. Blumberger, *J. Chem. Phys.*, 2010, **133**, 244105.
23 N. V. Plotnikov, S. C. L. Kamerlin and A. Warshel, *J. Phys. Chem. B*, 2011, **115**, 7950–7962.
24 H. Tamura, R. Martinazzo, M. Ruckenbauer and I. Burghardt, *J. Chem. Phys.*, 2012, **137**, 22A540.
25 H. Tamura and I. Burghardt, *J. Am. Chem. Soc.*, 2013, **135**, 16364–16367.
26 H. Tamura and I. Burghardt, *J. Phys. Chem. C*, 2013, **117**, 15020–15025.
27 C. T. Chapman, W. Liang and X. Li, *J. Phys. Chem. A*, 2013, **117**, 2687–2691.
28 In principle, a huge diversity of C_{60}–hexapyropheophorbide-*a* likewise molecular structures could be alternatively synthesized, for instance, based on more usual porphyrins instead of the pyropheophorbide-*a* molecules. However, the here reported C_{60}–hexapyropheophorbide-*a* adduct was initially designed for drug delivery in the field of the photodynamic therapy.[29] Thereby, in our cooperating experimental group (Röder *et al.*), the pyropheophorbide-*a* molecule was commonly used as the photosensitizer.
29 M. Regehly, E. A. Ermilov, M. Helmreich, A. Hirsch, N. Jux and B. Röder, *J. Phys. Chem. B*, 2007, **111**, 998–1006.
30 H. Imahori and T. Umeyama, *J. Phys. Chem. C*, 2009, **113**, 9029–9039.
31 J. Megow, T. Plehn, R. Steffen, B. Röder and V. May, *Chem. Phys. Lett.*, 2013, **585**, 178–183.
32 J. Megow, B. Röder, A. Kulesza, V. Bonačić-Koutecký and V. May, *ChemPhysChem*, 2011, **12**, 645–656.
33 R. A. Marcus, *J. Chem. Phys.*, 1956, **24**, 966–978.
34 A. Weller and D. Rehm, *Isr. J. Chem.*, 1970, **8**, 259–271.
35 B.-R. Hyun, A. C. Bartnik, L. Sun, T. Hanrath and F. W. Wise, *Nano Lett.*, 2011, **11**, 2126–2132.
36 C. Leng, H. Qin, Y. Si and Y. Zhao, *J. Phys. Chem. C*, 2014, **118**, 1843–1855.
37 H. Zhu, V. May, B. Röder and T. Renger, *J. Chem. Phys.*, 2008, **128**, 154905.
38 H. Zhu, V. May and B. Röder, *Chem. Phys.*, 2008, **351**, 117–128.
39 J. Megow, Y. Zelinskyy, B. Röder, A. Kulesza, R. Mitrić and V. May, *Chem. Phys. Lett.*, 2012, **522**, 103–107.
40 N. L. Doltsinis and D. Marx, *Phys. Rev. Lett.*, 2002, **88**, 166402.
41 M. E. Madjet, A. Abdurahman and T. Renger, *J. Phys. Chem. B*, 2006, **110**, 17268–17281.
42 A. Osuka, Y. Wada and S. Shinoda, *Tetrahedron*, 1996, **52**, 4311–4326.
43 T. F. Guarr, M. S. Meier, V. K. Vance and M. Clayton, *J. Am. Chem. Soc.*, 1993, **115**, 9862–9863.
44 I. R. Gould, D. Ege, J. E. Maser and S. Farid, *J. Am. Chem. Soc.*, 1990, **112**, 4290–4301.
45 M. Tachiya, *J. Chem. Phys.*, 1993, **97**, 5911–5916.
46 I. R. Gould, R. H. Young, R. E. Moody and S. Farid, *J. Phys. Chem.*, 1991, **95**, 2068–2080.
47 V. May and O. Kühn, *Charge and Energy Transfer Dynamics in Molecular Systems*, Wiley-VCH, 3rd edn 2011.
48 A. Heck, P. Woiczikowski, T. Kubař, B. Giese, M. Elstner and T. Steinbrecher, *J. Phys. Chem. B*, 2012, **116**, 2284–2293.
49 F. De Angelis, G. Vitillaro, L. Kavan, M. K. Nazeeruddin and M. Grätzel, *J. Phys. Chem. C*, 2012, **116**, 18124–18131.
50 D. M. Guldi, C. Luo, M. Prato, A. Troisi, F. Zerbetto, M. Scheloske, E. Dietel, W. Bauer and A. Hirsch, *J. Am. Chem. Soc.*, 2001, **123**, 9166–9167.

51 A. D. Becke, *Phys. Rev. A: At., Mol., Opt. Phys.*, 1988, **38**, 3098–3100.
52 M. J. Frisch and *et al.*, *Gaussian 09 Revision D.01, 2009*, Gaussian Inc., Wallingford CT, 2009.
53 C. M. Breneman and K. B. Wiberg, *J. Comput. Chem.*, 1990, **11**, 361–373.
54 H. Zhu, V. May, B. Röder, M. E.-A. Madjet and T. Renger, *Chem. Phys. Lett.*, 2007, **444**, 118–124.
55 J. Megow, A. Kulesza, Z. Qu, T. Ronneberg, V. Bonačić-Koutecký and V. May, *Chem. Phys.*, 2010, **377**, 10–14.
56 D. A. Case, *AMBER 8*, University of California, San Francisco, CA, 2004.
57 J. C. Phillips, R. Braun, W. Wang, J. Gumbart, E. Tajkhorshid, E. Villa, C. Chipot, R. D. Skeel, L. Kal and K. Schulten, *J. Comput. Chem.*, 2005, **26**, 1781–1802.
58 W. D. Cornell, P. Cieplak, C. I. Bayly, I. R. Gould, K. M. Merz, D. M. Ferguson, D. C. Spellmeyer, T. Fox, J. W. Caldwell and P. A. Kollman, *J. Am. Chem. Soc.*, 1995, **117**, 5179–5197.
59 J. Wang, R. Wolf, J. Caldwell, P. Kollman and D. Case, *J. Comput. Chem.*, 2004, **25**, 1157–1174.
60 M. G. Paterlini and D. M. Ferguson, *Chem. Phys.*, 1998, **236**, 243–252.
61 G. J. Martyna, D. J. Tobias and M. L. Klein, *J. Chem. Phys.*, 1994, **101**, 4177–4189.